Miniaturized Polarization Conversion Metasurface for RCS Reduction

Xiwang Dai[1, 2], Ningqi Tang[1], Ze Li[1], Wenhao Hu[1], and Hui Hong[1]

[1]School of Electronic Information
Hangzhou Dianzi University, Hangzhou 310018, China
xwdai@hdu.edu.cn, 2669397247@qq.com, 1223406727@qq.com, 2274714528@qq.com, hongh@hdu.edu.cn

[2]State Key Laboratory of Millimeter Waves
Southeast University, Nanjing 210096, China

Abstract – In this study, a miniaturized polarization conversion metasurface (PCM) with a cell size of 6×6 mm is utilized to reduce the radar cross-section (RCS) of a circularly polarized antenna array. Each cell circuit of the PCM comprises a pair of folded L-shaped strips with a meander line, which are printed on the surface of the substrate. This configuration demonstrates a polarization rotation (PR) bandwidth of 112% and achieves a high polarization conversion ratio (PCR) of 90%. To confirm the efficacy of the RCS reduction, the PCM is integrated with a circularly polarized 2×2 dipole antenna array. The measured results of the array are in excellent agreement with the simulated data, indicating at least a 5 dB reduction in monostatic RCS for the proposed antenna array. Furthermore, the integration of the PCM does not degrade the radiation performance of the antenna array, confirming the PCM's suitability for RCS reduction without compromising antenna functionality.

Index Terms – Circularly polarized dipole antenna array, miniaturized, PCM, RCS.

I. INTRODUCTION

An antenna can not only radiate/receive electromagnetic waves, but also scatter electromagnetic waves as a special structure, which greatly increases the radar cross-section (RCS) of the antenna and seriously affects its application in safe communication. Developing an antenna that can achieve both ultra-wideband low RCS and wideband radiation is of great significance and necessity [1, 2].

Reflective polarization rotators have received considerable attention in the development of stealth platforms [3]. Linear-to-linear rotating polarization conversion metasurface (PCM) designs that use asymmetric elements can achieve a phase difference of 180°, making them suitable for stealth platforms [4–5].

Metasurface-based polarization rotators have the advantage of being compact and lightweight, making them highly suitable for antenna RCS reduction [6–9]. For example, a sawtooth polarization conversion metasurface operating in the terahertz (THz) band has been proposed [6]. A PCM positioned at an appropriate height above a coil can form a Fabry-Perot cavity to enhance gain [7]. An RCS reduction of circularly polarized antennas has been achieved using circular polarization conversion electromagnetic band-gap (CPC EBG) structures [8], while an improvement to the conventional L-shaped strip in a tapered strip design has expanded the polarization rotation bandwidth of PCM units to 117.2% [9]. Moreover, the antennas developed using this method often require multi-layer structures, whereby controlling the area of the metasurface can be difficult. Several methods are proposed for broadband RCS reduction, such as a dartboard-shaped layout [10], rotated phase coding phase [11], and two-layer stacked resonance absorber [12]. Based on the hybrid mechanism metasurface of the Panchartnam–Berry phase, a 2×2 array is proposed for 2∼13 GHz low RCS in [13]. However, these unit cells need complex multilayers or large size, which limit their application in antenna array.

A novel approach for reducing the RCS of a circular polarized dipole antenna, using a miniaturized PCM, has been presented in this paper. The meander lines are applied to the arms of L-shaped strip, which can greatly reduce the resonant frequency. Electromagnetic (EM) simulation and equivalent circuit are conducted for the performance and working mechanism of miniaturized cell. A 2×2 array with circularly polarization is integrated with PCM to validate the effect of RCS reduction.

II. THEORY OF THE PCM

A. Structure of PCM cell

The detailed parameters are given in Fig. 1. The substrate is F4B with a relative dielectric constant of ε_r =2.2, tanδ =0.0009, and a height of 4 mm. When the electromagnetic wave is incident on the cell, the folded part can provide a longer current path, thus realizing the miniaturization of the cell. We use a Floquet Port to simulate a periodic arrangement of the PCM cell. The overall

Submitted On: March 10, 2024
Accepted On: March 14, 2025

https://doi.org/10.13052/2024.ACES.J.400303

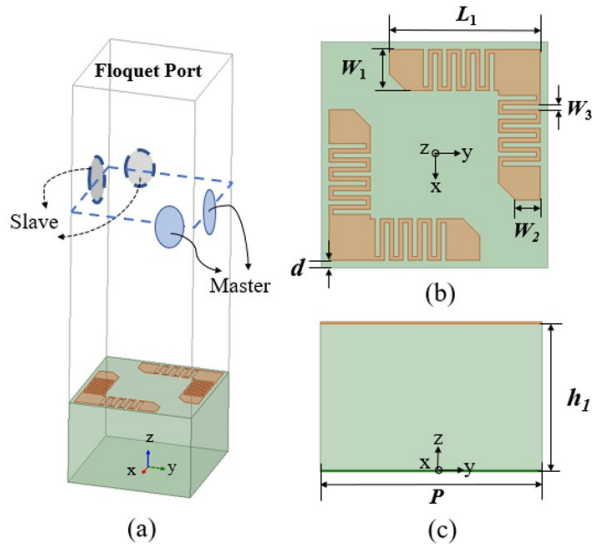

Fig. 1. Structure of the proposed PCM cell: (a) overall view, (b) top view and (c) side view.

structure was simulated and analyzed with the software of HFSS with the following optimized parameters: P=6, h_1 =4, L_1 =4, W_1 =1.1, W_2=0.44, W_3 =0.13, d=0.2, all units being in mm.

B. Design procedure

Polarization conversion ratio (PCR) is a key indicator to measure the ability of different polarization waves to be converted. It is defined as PCR=$|\Gamma_{xy}|^2/(|\Gamma_{xy}|^2+|\Gamma_{yy}|^2)$ to demonstrate the ability to convert when an y-polarized linear polarization (LP) incident wave to an x-polarized reflected wave. Here, $|\Gamma_{yy}|$ denotes the reflection coefficient of a y-polarized incident wave to a y-polarized reflected wave. Similarly, $|\Gamma_{xy}|$ denotes the reflection coefficient of a y-polarized incident wave to an x-polarized reflected wave.

The PCM cell iterative design from Model 1 to Model 4 shown in Fig. 2. A Floquet Port has been used to simulate a periodic arrangement of the models. The corresponding PCR values for each model, can be depicted from Fig. 3. Initially, Model 1 employs a L-shaped metallic strip with PCR greater than 0.9 at a narrow frequency band range of 20.1-20.9 GHz. Subsequently, another same strip is added and placed diagonally opposite the original shape. However, Model 2 exhibits a shift in the operating frequency towards lower frequencies and a resonant frequency in the PCR curve. Moreover, in the middle band, the PCR performance of Model 2 deteriorates. To address this problem, the interior of the patch is folded to create Model 3, which resonates in the middle frequency band. Although Model 3 enhances the PCR performance slightly at low and high frequencies, there is a band of poor results in the middle frequencies. Moreover, another resonant frequency occurs at 11.2 GHz. Finally, the number of times the patch is folded internally is optimized to achieve the best PCR performance for Model 4. In the entire broadband frequency range of 6.2-18.5 GHz, Model 4 exhibits excellent PCR performance, which is greater than 0.9. In particular, at four frequency points (6.6, 10.3, 16.3, and 17.7 GHz) the PCR assumes values close to 1.0, indicating that the proposed PCM achieves a phase of 90° rotation of polarization.

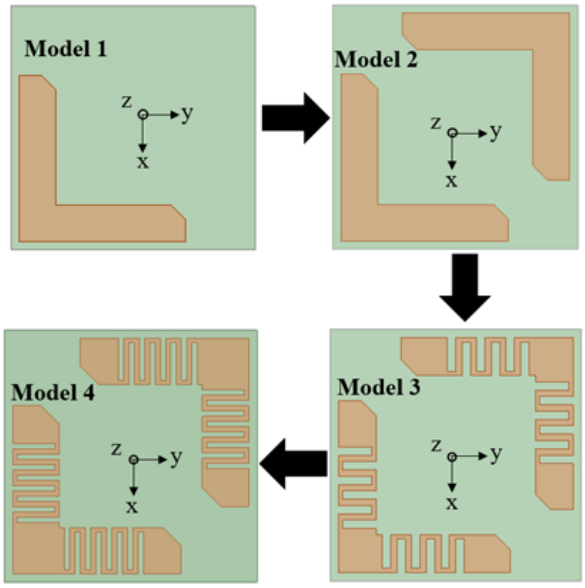

Fig. 2. Iterative design process of the PCM cell.

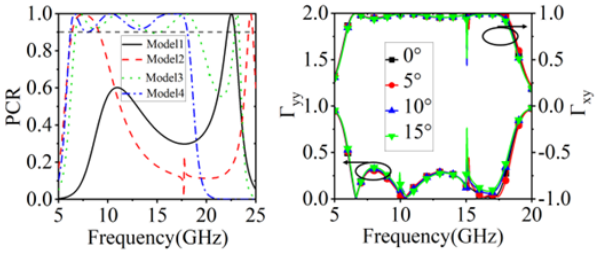

Fig. 3. Simulated performance of the PCM cell: (a) PCR of each model and (b) reflection coefficients of y-polarized incident wave.

Simulated magnitudes of the reflection coefficients $|\Gamma_{yy}|$ and $|\Gamma_{xy}|$ with y-polarized incident waves at different oblique angles are shown in Fig. 3 (b). $|\Gamma_{xy}|$ tends to deteriorate in specific frequency band as θ increases. The origins of the spikes are mainly caused by some self resonance generated by L-shaped strip with metal ground. When electromagnetic waves are obliquely incident on

a cell, its folded lines no longer maintain their original inductance values; At the same time, the capacitance between the patch and the metal ground will also change. This leads to the appearance of spikes in the reflection coefficient.

C. Theoretical analysis

The L-shaped branch has two perpendicular arms that alter the polarization of the resonant electromagnetic waves on it. The anisotropy of the PCMs and the near-field variation caused by interference can be adjusted to control the polarization of the final reflected wave. Figure 4 (a) shows the electric field of an incident wave along the u-axis and v-axis directions, which can be expressed as:

$$\vec{E}^{i} = \hat{a}_u E_u^i e^{j\varphi_u} + \hat{a}_v E_v^i e^{j\varphi_v}. \quad (1)$$

The reflected wave can be expressed with reflection coefficients, where λ_u and λ_v are the reflection coefficients for the u and v axes:

$$\vec{E}_r^{i} = \hat{a}_u \lambda_u E_u^r e^{j\varphi_u} + \hat{a}_v \lambda_v E_v^r e^{j\varphi_v}. \quad (2)$$

Depending on those equations, the polarization of the incident wave will rotate by 90° when $\lambda_u = \lambda_v$ and the phase difference between the two reflected waves is $\Delta\varphi = 180°$. The reflection magnitude for the u and v axes are given in Fig. 4 (b).

To elucidate the underlying mechanism responsible for the polarization rotation (PR), the surface current distributions at the four resonant frequencies of the PCM cell are presented in Fig. 5. It is observed that the current intensity at both ends and in the middle of the two metal patches are relatively weak, whereas a strong current flows along both sides of the folding slit within the patch. Consequently, in this configuration, the folded structure can be conceptualized as a patch resonator, which establishes a current loop that induces magnetic resonance.

An equivalent circuit is constructed to explain the working mechanism of PCM, as shown in Fig. 6. The PCM is equivalent to two LC series circuits representing

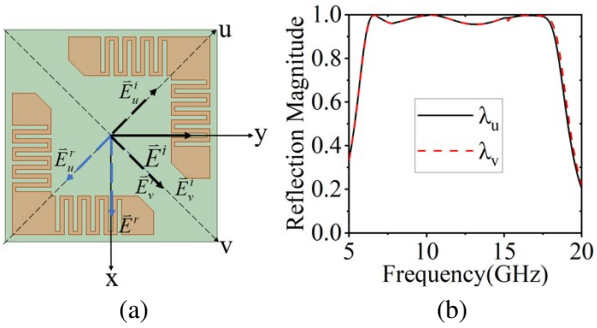

Fig. 4. PCM cell performance analysis under oblique polarization: (a) u- and v-field component and (b) reflection magnitude along u- and v-axis.

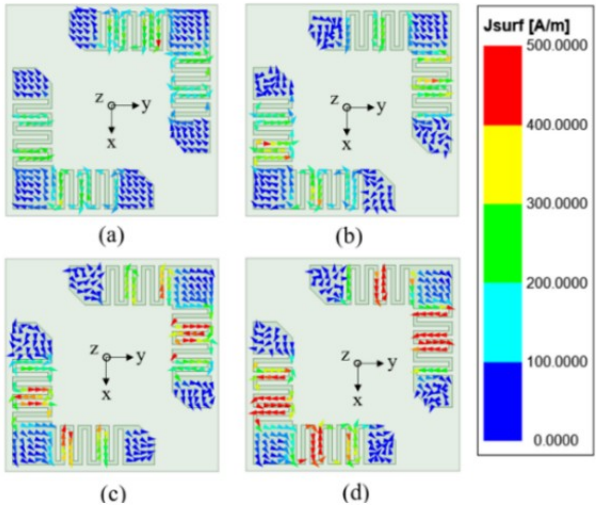

Fig. 5. Simulated surface current of the PCM unit at (a) 6.6 GHz, (b) 10.3 GHz, (c) 16.3 GHz, and (d) 17.7 GHz.

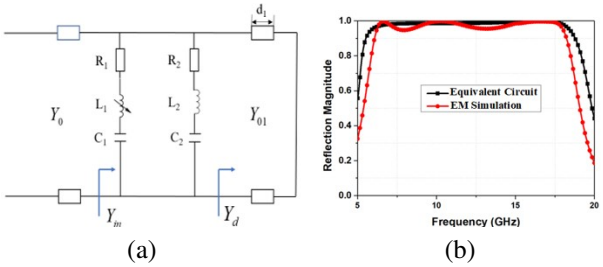

Fig. 6. Equivalent circuit of the proposed PCM: (a) circuit and (b) performance.

the metal patch and the coupling between the two metal patches. The resistance is introduced for the loss when the frequency of electromagnetic wave is not within the working frequency band . An adjustable inductor is used to represent the meander line of the L-shaped strip. The dielectric layer is represented by a transmission line with a length of d_1, and the reflector plate is represented by a short on the right. Y_0 represents the characteristic conductance of air and the reflection coefficient can be written as $\Gamma = (Y_0 - Y_{in})/(Y_0 + Y_{in})$, the conductances of two LC series circuits are labeled as Y_L, Y_{L2}, respectively. Then:

$$Y_{in} = Y_{L_1} + Y_{L_2} + Y_d, \quad (3)$$

$$Y_{L_1} = \frac{1}{R_1 + j\left(\omega L_1 - \frac{1}{\omega C_1}\right)}, \quad (4)$$

$$Y_{L_2} = \frac{1}{R_2 + j\left(\omega L_2 - \frac{1}{\omega C_2}\right)}, \quad (5)$$

$$Y_d = -jY_{01} d_1 \tan\beta. \quad (6)$$

The values of lumped elements in the equivalent circuit are given: $R_1 = 10\Omega$, $L_1 = 12.5$ nH, $C_1 = 0.076$

pF, R_2 =9Ω, L_2 = 1.02 nH, C_2 = 0.049 pF. With these parameters, the equivalent circuit is simulated with AWR Design Environment, and the corresponding results are added to Fig. 6 (b). The performance of equivalent circuits and electromagnetic simulation have good consistency throughout the entire frequency band.

III. CP DIPOLE ANTENNA ARRAY

A. Antenna element

The antenna element adopts the classic dipole with meander line arm to achieve compact size, as shown in Fig. 7. The dipole is placed above a PCM plane with 5×5 cells and supported by a F4B substrate with a height of 1 mm.

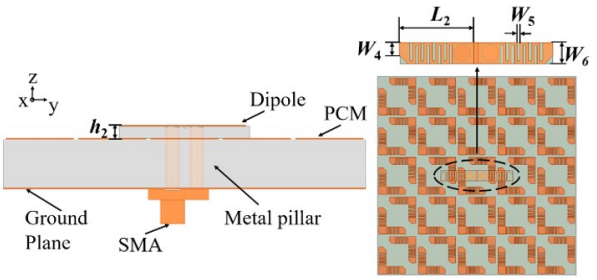

Fig. 7. Structure of the antenna with PCM: (a) side view and (b) vertical view with the parameters of L_2 =5.3 mm, W_4 =0.9 mm, W_5=0.2 mm, W_6 =1.5 mm, h_2 =1 mm.

The performance of the antenna element is shown in Figs. 8 (a) and (b). The 3 dB axial ratio (AR) band covers 6.5 GHz to 7.5 GHz. The AR values within the impedance band of 6.87 to 7.35 GHz are all less than 3 dB. The antenna exhibits circular polarization characteristics throughout the band.

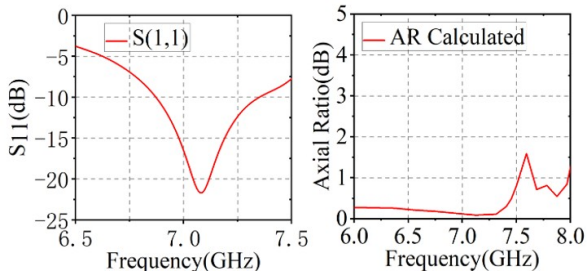

Fig. 8. Simulated results: (a) reflection coefficient and (b) AR of dipole with PCM.

B. Antenna array

The four antenna units are sequentially rotated by 90° and arranged in a checkerboard configuration to form the array antenna. The reference array antenna, designated as Array 1, consists of four dipole cells that are rotated and combined as depicted in Fig. 9 (a). Each dipole is oriented in a manner that facilitates center-fed rotation, thereby enhancing circular polarization (CP) performance. The energy field from the port is evenly fed into the dipole antenna array through a one-to-four power divider as the feed network, which shares a common ground layer with the PCM plane.

The designed tessellated PCM is placed beneath the antenna to decrease its RCS. The final design structure, called Array 2, is shown in Fig. 9 (b). The structure comprises a dipole array, a substrate printed PCM coating, and a feed network. To verify the design structure, Arrays 1 and 2 were fabricated in Fig. 10 and the measured environment is shown in Fig. 11.

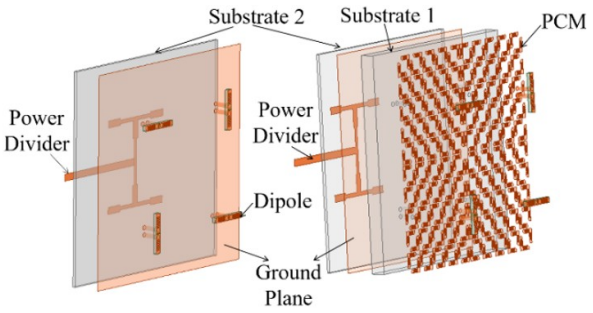

Fig. 9. Exploded view of antenna array: (a) Array 1 without PCM and (b) Array 2 with PCM.

Fig. 10. Photograph of antenna array: (a) Array 1 without PCM and (b) Array 2 with PCM.

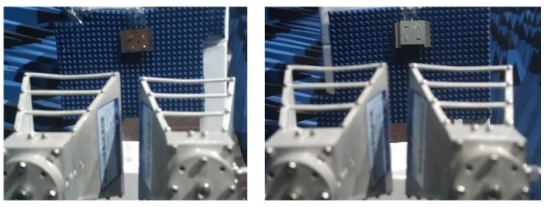

Fig. 11. Measured environment of antenna array: (a) Array 1 without PCM and (b) Array 2 with PCM.

C. Simulation and measurement

To verify the performance of the proposed structure, Arrays 1 and 2 were fabricated, measured, and compared. A comparison of S11 of the simulated and measured arrays is provided in Fig. 12. It can be seen that the simulated working frequency bands of Array 1 extends from 6.85 to 7.02 GHz for $|S11| \leq$ -10 dB. The impedance bandwidth ranges from 6.82 to 7.12 GHz for Array 2. The bandwidth of the antenna is slightly broadened by addition of the PCM, due to the antenna being influenced by the surface electric field excited by the PCM. The measured bandwidth ranges from 6.86 to 7.12 GHz for Array 1 and 6.98 to 7.09 GHz for Array 2, respectively. The measured operating frequency was excursed by approximately 0.1 GHz towards the high frequencies while the trends remained constant.

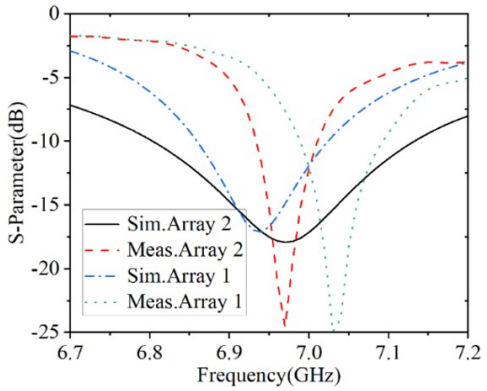

Fig. 12. Performance of Arrays 1 and 2.

Figure 13 shows the simulated and measured radiation patterns for Arrays 1 and 2 at 7.125 GHz. The simulated achieved gains are 11.356 dBi (Array 1) and 12.402 dBi (Array 2), respectively. Loading the PCM increases the gain of the ports by 1.0 dBi each. The measured actual gain is about 0.6 dBi less than the simulated gain in the XZ- and YZ-planes, respectively. This difference is mainly due to the loss of connector and manufacturing accuracy. The simulated and measured curves are in good agreement. Stable directional CP radiations with PCM coating are achieved. A high degree of isolation is achieved between the co-polarized and cross-polarized radiation on the aiming line.

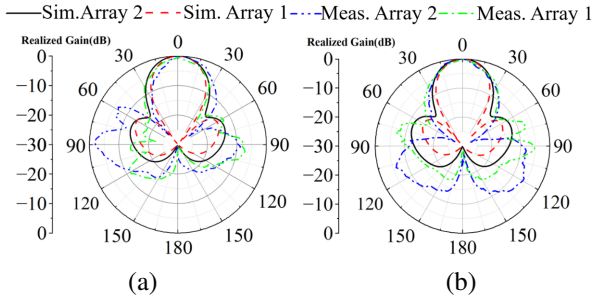

Fig. 13. Simulated and measured radiation patterns: (a) XZ-plane and (b) YZ-plane at 7.125 GHz.

Figure 14 shows the simulated and measured monostatic RCS reduction curves for Arrays 1 and 2 for x- and y-polarizations at normal incidence. The IncPWave Port of HFSS is used to simulate the general incident wave to obtain the simulation results of the metasurface. The simulated 5 dB RCS reduction scaling bandwidths for both polarizations are between 6.1 GHz and 20.7 GHz, which covers the operating band of the antenna. The measured 5 dB RCS reduction scaling bandwidths are from 6.1 GHz to 20.8 GHz and 6.2 GHz to 21.9 GHz (x-polarization) and 5.9 GHz to 20.7 GHz and 6.2 GHz to 22 GHz (y-polarization).

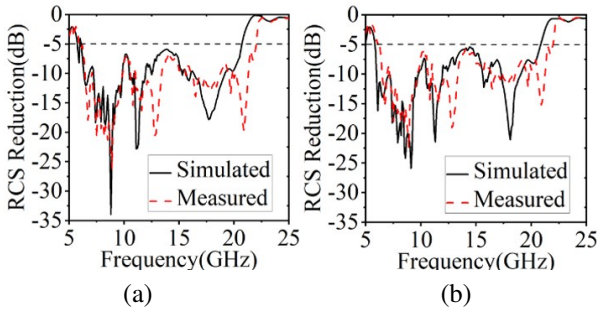

Fig. 14. RCS reduction of the arrays: (a) x-polarization and (b) y-polarization.

The simulated 3D bistatic RCS of Arrays 1 and 2 at 8.0 GHz under normal incidence x-polarization wave are shown in Fig. 15. Given that the reflection amplitudes are equivalent, the phase difference between the mirror cells is 180° following the checkerboard arrangement, resulting in mutual cancellation that diminishes the scattered energy in the +z direction. Concurrently, the superpo-

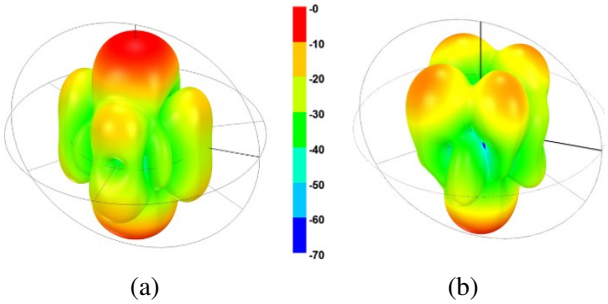

Fig. 15. 3-D bistatic RCS of the array at 8 GHz under x-polarization incidence for (a) Array 1 and (b) Array 2.

Table 1: Comparison between other work and this work

Ref.	Electric Size ($\lambda_0 \times \lambda_0$)	No. of PCM Unit	Impedance Matching BW (GHz)	Type of Reduction	Polarization	RCS Reduction BW (GHz)
[7]	1.41×1.41	4×4	9.5-11.6	In-band Out-of-band	Single LP	7.5-17.1 (78.0%)
[8]	0.90×0.90	4×4	4.8-7	In-band Out-of-band	CP	4.7-5.8 (21.0%)
[9]	1.76×1.76	7×7	6.06-6.75/ 6.28-6.47	Out-of-band	Dual LP	9.6-33.1(110.0%) 9.8-33.2(110.0%)
This work	**0.71×0.71**	**5×5**	**6.87-7.35**	**In-band Out-of-band**	**CP**	**6.1-20.7 (109.2%)**

sition of the reflected waves gives rise to four subdued scattering peaks.

A performance comparison between our work with other low-RCS antennas is listed in Table 1. As can be seen from the comparison, the model in reference [7] has ultra-wide impedance matching bandwidth, and its RCS reduction also reaches 78% bandwidth, but it is only applied in single-line polarization, and its electrical size is large. A miniaturized cell has been proposed and applied for RCS reduction [8]; however, its operating bandwidth is only 21%. A model with an RCS reduction bandwidth of up to 110% was proposed in [9], which demonstrated excellent working frequency band and dual line polarization operation, but the cell needs complex multilayers. The proposed antenna achieves a small size of $0.71\lambda_0 \times 0.71\lambda_0$ and the characteristics of miniaturization are obvious. Meanwhile, the RCS of this antenna is reduced in a broadband frequency range 6.1-20.7 GHz (109.2%) with 5 dB reduction and includes the working frequency band of the antenna.

IV. CONCLUSION

A low RCS, gain-enhanced, miniaturized CP array is presented in this paper. A folded ultra-wideband PCM is designed and applied as the coating of the array. The low-profile CP radiation is achieved through a tessellated PCM plane, which reduces the RCS of the array by 5 dB RCS in the range 6.1-20.7 GHz (109.2%). The PCM area used for the single antenna is only 30×30 mm ($0.71\lambda o \times 0.71\lambda o$), a significant miniaturization feature. The performance of the array is investigated by simulation and testing.

ACKNOWLEDGMENT

This work is supported partly by "Pioneer" and "Leading Goose" R&D program of Zhejiang under contract of 2022C01119, partly by the National Natural Science Foundation of China under Contract of 62171169, partly by Project of State Key Laboratory of Millimeter Waves under contract of K202414.

REFERENCES

[1] T. Liu, X. Y. Cao, J. Gao, Q. Zheng, W. Li, and H. Yang, "RCS reduction of waveguide slot antenna with metamaterial absorber," *IEEE Trans. Antennas Propag*., vol. 61, no. 3, pp. 1479-1484, Mar. 2013.

[2] Y. Q. Li, H. Zhang, Y. Q. Fu, and N.-C. Yuan, "RCS reduction of ridged waveguide slot antenna array using EBG radar absorbing material," *IEEE Antennas Wireless Propag. Lett.*, vol. 7, pp. 473-476, 2008.

[3] H. B. Wang, Y. J. Cheng, and Z. N. Chen, "Wideband and wide-angle single-layered-substrate linear-to-circular polarization metasurface converter," *IEEE Trans. Antenna Propag*., vol. 68, no. 2, pp. 1186-1191, Feb. 2020.

[4] K. K. Chan, "Ultra-wide band variable linear polarization rotator with high cross-polarization discrimination for scanned beams," *IEEE International Symposium on Antennas and Propagation and USNC-URSI Radio Science Meeting (APS/URSI)*, Singapore, pp. 983-984, 2021.

[5] Meraj-E-Mustafa, R. Izhar, M. S. Wahidi, F. A. Tahir, and Q. H. Abbasi, "A broadband 90° polarization rotator metasurface," *International Conference on Microwave and Millimeter Wave Technology (ICMMT)*, Shanghai, China, pp. 1-2, 2019.

[6] Deepti, D. Gangwar, S. Singh, A. Sharma, and M. R. Tripathy, "Design of terahertz PCM and its application in polarisation conversion and RCS reduction," *IEEE Indian Conference on Antennas and Propagation (InCAP)*, Jaipur, Rajasthan, India, pp. 863-866, 2021.

[7] X. Liu, E. Wang, X. Geng, D. Yang, and Z. Yan, "Broadband RCS reduction for Fabry-Perot antenna with enhanced bandwidth using polarization conversion metasurface," *International Symposium on Antennas and Propagation (ISAP)*, Osaka, Japan, pp. 773-774, 2021.

[8] Q. Zheng, C. Guo, G. A. E. Vandenbosch, and J. Ding, "Low-profile circularly polarized array with gain enhancement and RCS reduction using polarization conversion EBG structures," *IEEE Trans. Antennas Propag.*, vol. 68, no. 3, pp. 2440-2445, Mar. 2020.

[9] J. Liu, J.-Y. Li, and Z. N. Chen, "Broadband polarization conversion metasurface for antenna RCS reduction," *IEEE Trans. Antenna Propag.*, vol. 70, no. 5, pp. 3834-3839, May 2022.

[10] W. Geng and Q. Guo, "Design of a dartboard metasurface for broadband RCS reduction," in *2023 IEEE 11th Asia-Pacific Conference on Antennas and Propagation (APCAP)*, Guangzhou, China, pp. 1-2, 2023.

[11] G.-Y. Deng, Y.-H. Zhang, H.-T. Gao, Y.-L. Shu, and G.-Q. Zhu, "A super diffuse broadband RCS reduction surface design based on rotated phase coding polarization conversion metasurfaces," *IEEE Transactions on Antennas and Propagation*, vol. 71, no. 9, pp. 7409-7417, Sep. 2023.

[12] D.-X. Song, S.-F. Wang, W.-J. Liao, and Y.-C. Hou, "Homogeneous two-layer structures for broadband and wide-angle RCS reduction," *IEEE Antennas and Wireless Propagation Letters*, vol. 22, no. 5, pp. 1074-1078, May 2023.

[13] L. Zhu, J. Sun, Z. Hao, X. Kuai, H. Zhang, and Q. Cao, "A broadband low-RCS antenna based on hybrid mechanism metasurface," *IEEE Antennas and Wireless Propagation Letters*, vol. 22, no. 5, pp. 975-979, May 2023.

Xiwang Dai was born in Caoxian, Shandong, China. He received the B.S. and M.S. degrees in electronic engineering from Xidian University, Xi'an, Shaanxi, China, in 2005 and 2008, respectively. Dai received the Ph.D. degree in electromagnetic fields and microwave technology from Xidian University in 2014. From March 2008 to August 2011, he worked at Guangdong Huisu Corporation as a manager of the antenna department. Presently, he is working at the Hangzhou Dianzi University, Hangzhou, China. His current research interests involve broadband antenna, RCS and metasurface.

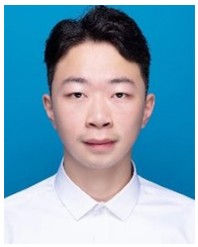

Ningqi Tang was born in Yongzhou, Hunan, China. He received the B.S. degree in electronic engineering from Nanchang University, Nanchang, Jiangxi, China, in 2021. Presently, he is studying for the M.S. degree at Hangzhou Dianzi University, Hangzhou, China. His current research interests include broadband antenna and low-RCS antenna.

Ze Li was born in Wenzhou, Zhejiang, China. He received the B.S. degree in electronic engineering from Hangzhou Dianzi University Information Engineering College, Hangzhou, China, in 2023. Presently, he is studying for the M.S. degree at the Hangzhou Dianzi University, Hangzhou, China. His current research interests include transmitarray antenna and reflectarray antenna.

Wenhao Hu was born in Zoucheng, Shandong, China. He received the B.S. degree in Electronic Information Engineering from Shandong Technology and Business University, Yantai, Shandong, China, in 2022. Presently, he is studying for the M.S. degree at the Hangzhou Dianzi University, Hangzhou, China. His current research interests include MIMO antenna and array antenna decoupling.

Hui Hong received the Ph.D. degree from the College of Information Science and Electronic Engineering, Zhejiang University, Hangzhou, China, in 2007. He is currently a Full Professor at the School of Electronics and Information Engineering, Hangzhou Dianzi University, Hangzhou. His current research interests include brain-computer interface, microsystem integration and biological signal processing.